JOURNAL OF GEOPHYSICAL RESEARCH, VOL. 98, NO. A4, PAGES 5839–5853, APRIL 1, 1993

The Nonlinear Evolution of Field Line Resonances in the Earth's Magnetosphere

R. RANKIN, B. G. HARROLD, J. C. SAMSON, AND P. FRYCZ

Canadian Network for Space Research, University of Alberta, Edmonton, Alberta, Canada

Magnetohydrodynamic, field line resonances in the Earth's magnetosphere can have very large velocity shears and field-aligned currents. Auroral radar measurements of high-latitude resonances indicate that the velocities associated with the resonances in the *E* and *F* regions are often substantially greater than 1 km/s, and that the frequencies are in the interval from 1 to 4 mHz. Assuming that these resonances are oscillating at the fundamental mode frequency, and mapping these velocity fields along magnetic field lines to the equatorial plane shows that the velocity shears in the equatorial plane are of the order of 200 km/s over a radial distance of less than 2000 km (the amplitude of the velocity fluctuations is 100 km/s). Using a three-dimensional magnetohydrodynamic computer simulation code, we show that the resonances evolve through the development of Kelvin-Helmholtz instabilities near the equatorial plane. Within this framework, the instability is taking place on dipole magnetic field lines, and the resonances form a standing shear Alfvén wave field due to the boundary conditions which must be satisfied at the polar ionospheres. We find that the nonlinear evolution of the Kelvin-Helmholtz instability leads to the propagation of vorticity from the equatorial plane to the polar ionosphere and that the vorticity leads ultimately to the dissipation of the resonance. This occurs within a quarter wave period of the shear Alfvén field associated with the resonances.

INTRODUCTION

The coupling of compressional, magnetohydrodynamic (MHD) waves to shear Alfvén waves leads to the formation of field line resonances (FLRs) in the Earth's magnetosphere [*Southwood*, 1974, *Chen and Hasegawa*, 1974]. The growth of these resonances and the maximum amplitudes of the electric and magnetic fields within the resonances are limited by dissipation in the ionosphere [*Allan and Poulter*, 1989] and possibly by linear mode conversion to kinetic Alfvén waves or electron inertia waves [*Hasegawa*, 1976, *Goertz*, 1984]. *Hollweg and Yang* [1988] have also suggested that the velocity shear in Alfvén resonances might lead to the formation of Kelvin-Helmholtz instabilities (KHI), giving an effective eddy viscosity and dissipation of the MHD resonance. *Samson et al.* [1992a] have speculated that vortex structures in ionospheric *F* region flows associated with FLRs might be a manifestation of the nonlinear evolution of the FLR, leading to the KHI in the equatorial plane.

Much of the velocity shear in magnetospheric flows comes from large-scale magnetospheric convection, for example, within the low-latitude boundary layer. There is, however, a second mechanism for producing regions with strong shear and field aligned currents (FACs) in the inner magnetosphere. The coupling of compressional MHD wave energy to shear Alfvén waves in a nonuniform magnetoplasma gives oscillating vorticity and FACs within the magnetosphere [*Southwood*, 1974, *Chen and Hasegawa*, 1974], and forms FLRs on dipolelike field lines.These field line resonances are often seen in the high-latitude ionosphere [*Walker et al.*, 1979; *Ruohoniemi et al.*, 1991; *Samson et al.* 1992a]. In the equatorial plane of the magnetosphere, the fundamental mode of the FLRs has a perturbation magnetic field node and corresponding velocity field and electric field antinodes. At the conjugate ionospheres, the velocity and electric field have nodes and the wave magnetic field has an antinode. Thus the largest velocity shears occur on closed magnetic field lines in the equatorial plane of the magnetosphere. *Walker* [1980] has shown that the FLRs observed in the high-latitude *E* region of the ionosphere can have equatorial fluid velocities of the order of 80 km/s.

A class of very low frequency FLRs which are seen in the high-latitude ionosphere and magnetosphere have quantized frequencies of approximately 1.3, 1.9, 2.6, and 3.5 mHz. These resonances are thought to originate from the mode conversion of cavity mode compressional MHD waves. Compressional waves produced by the solar wind propagate antisunward in an MHD cavity which is produced by the waves reflecting from their turning points at the magnetopause and on dipole field lines close to the Earth [*Samson et al.*, 1992b]. A field line resonance is excited when the compressional wave couples to a shear Alfvén wave just Earthward of the turning points located on dipolar field lines; see Figure 1. The FLRs are seen on the nightside on field lines threading the auroral oval [*Samson et al.*, 1992a]. These nightside FLRs often have associated with them very strong velocity shears near the ionosphere, typically greater than 1 km/s in a 20- to 50-km latitudinal interval, and relatively large FAC, near $5\mu A\,m^{-2}$. The resonances often evolve into localized vortices, particularly during substorm intensifications [*Samson et al.*, 1992a]. Figure 2 shows observations of a vortex structure that grew within or near to a 1.3-mHz FLR situated at 70.5^0 latitude. On the diagram the velocity vectors are shown with the y axis representing magnetic north (latitude), and the x axis magnetic east (east magnetic longitude). The velocity map shows the view that would be seen in the northern hemisphere looking in the direction of the geomagnetic field. Using the FLR model presented by *Walker* [1980] we find that the velocity shear in the FLRs at the equatorial plane must be on the order of 200 km/s over a radial distance of less than 2000 km. These estimates for the velocity shear are also in close agreement with those of *Mitchell et al.* [1990], who observed FLRs associated with Pc 5 pulsations in data obtained during ISEE 1 and 2 satellite trajectories through the outer dawn magnetosphere. They located the FLRs at an equatorial radius of approximately $10.5R_E$ (consistent with estimates made by *Samson et al.* [1992a, b]) and identified periods for the waves of approximately 8 min. The vortices seen in the high-latitude

Paper number 92JA01606.
0148-0227/93/92JA-01606$05.00

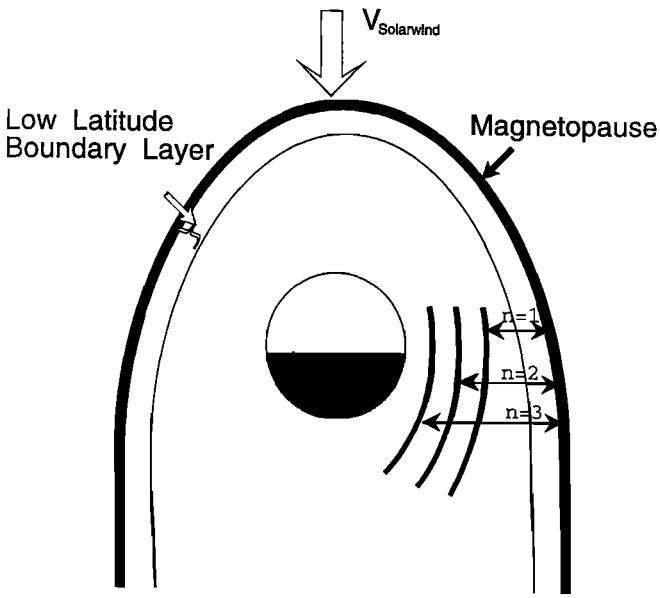

Fig. 1. The MHD waveguide in the equatorial plane of the Earth's magnetosphere. Mode convsion of compressional MHD waves to shear Alfvén waves couples energy to field line resonances at the positions indicated. The n=1, 2, 3 modes have frequencies of 1.3 mHz, 1.9 mHz and 2.6 mHz, respectively.

ionosphere may indicate that the FLRs are nonlinearly unstable. Possibilities include the nonlinear KHI [*Hollweg and Yang*, 1988] due to velocity shears near the equatorial plane, and unstable magnetic field shears near the ionosphere [*Hallinan*, 1976].

One aspect of auroral dynamics that the studies of these FLRs might help to clarify, concerns the vortex structures that are seen in plasma flows in the auroral regions and in auroral emissions. The auroral magnetosphere and ionosphere often have plasma flows in which strong shears and vorticity are present. These flows can lead to the dynamical evolution of vortex structures and localized vortex cells. For example, the vortex cell shown in Figure 2 was associated with a substorm intensification and the formation of an auroral surge [*Samson et al.*, 1992a, b]. This figure shows the evolution of *E* region flows as measured by the Canadian Bistatic Auroral Radar [*Samson et al.*, 1992b] just after the initiation of a substorm intensification. A 1.3-mHz FLR was situated at 70.5 degrees PACE latitude just prior to the breakup. The vortex cell in this example was observed to evolve out of the velocity fields associated with the FLR. Vortex structures are also seen in the form of curls, folds, and spirals in the ionospheric auroral forms produced by precipitating energetic electrons. *Hallinan and Davis* [1970] and *Davis and Hallinan* [1976] classified small-scale (order of 1 km) structures as curls, and large-scale structures (100 km or more) as spirals. *Hallinan* [1976] has suggested that curls may be formed in the velocity shears associated with auroral arcs, whereas spirals might be due to instabilities in current sheets. *Seyler* [1990] has considered the effects of finite electron inertia in the evolution of small-scale auroral structures and has concluded that collisionless tearing and reconnection of magnetic field lines might play a role in the evolution of these structures. A number of other plasma configurations can also lead to the nonlinear evolution of localized vortex structures. For example, *Shukla et al.* [1985] have shown that drift and shear Alfvén waves are coupled in a nonuniform magnetoplasma and that the nonlinear equations describing the coupling contain solitary vortex solutions.

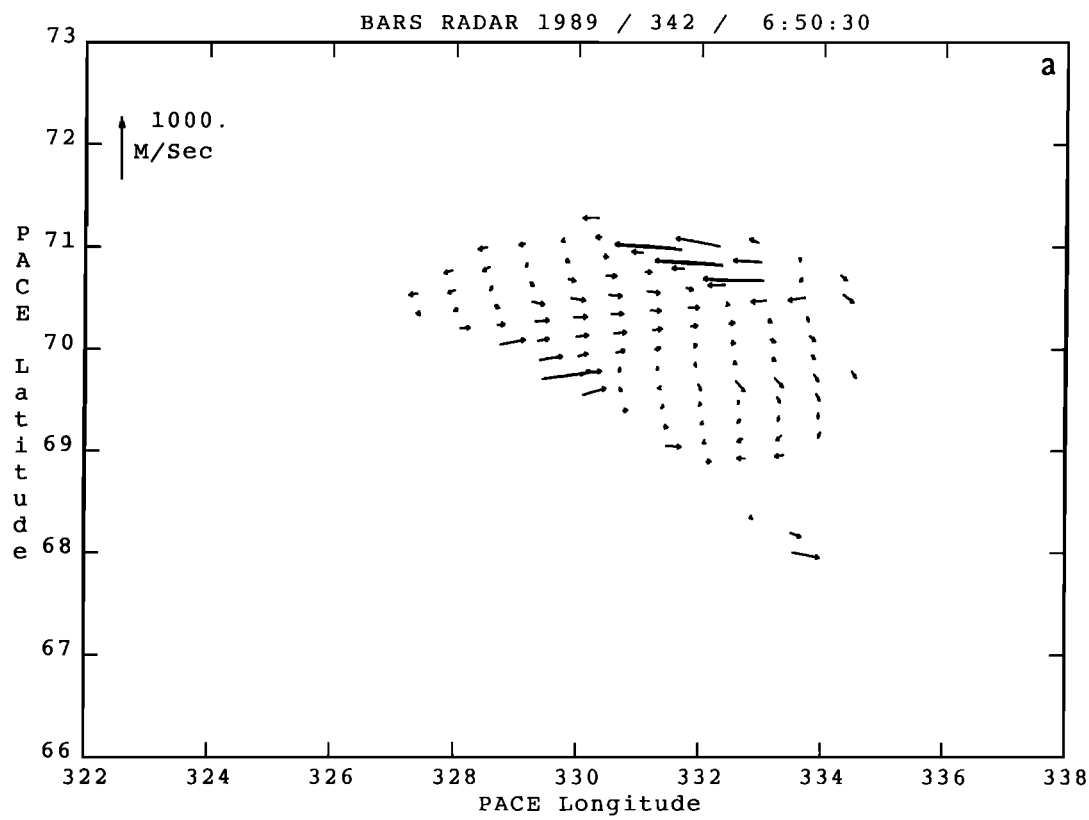

Fig. 2. *E* region drift velocities measured by the Canadian Bistatic Auroral Radar on December 8, 1989. The coordinates on the map are PACE geomagnetic coordinates [*Baker and Wing*, 1989]. (a) 0650:30 UT, (b) 0651:00 UT, and (c) 0651:30 UT.

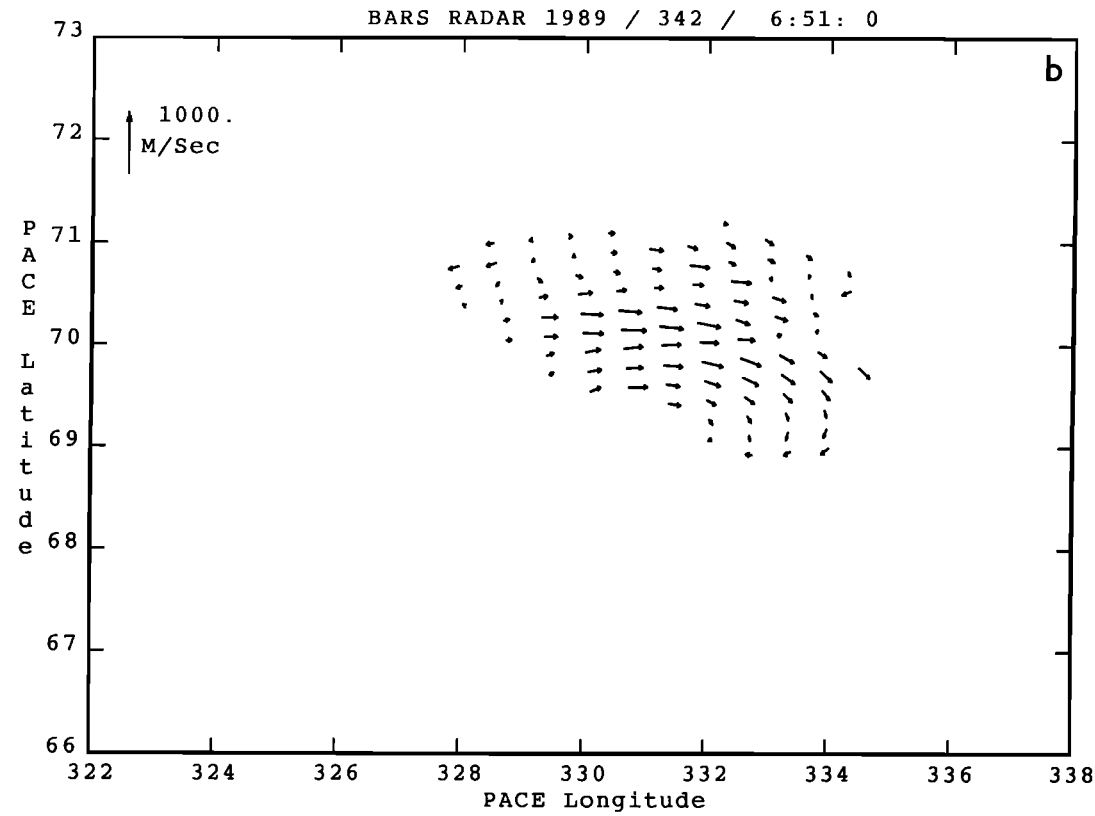

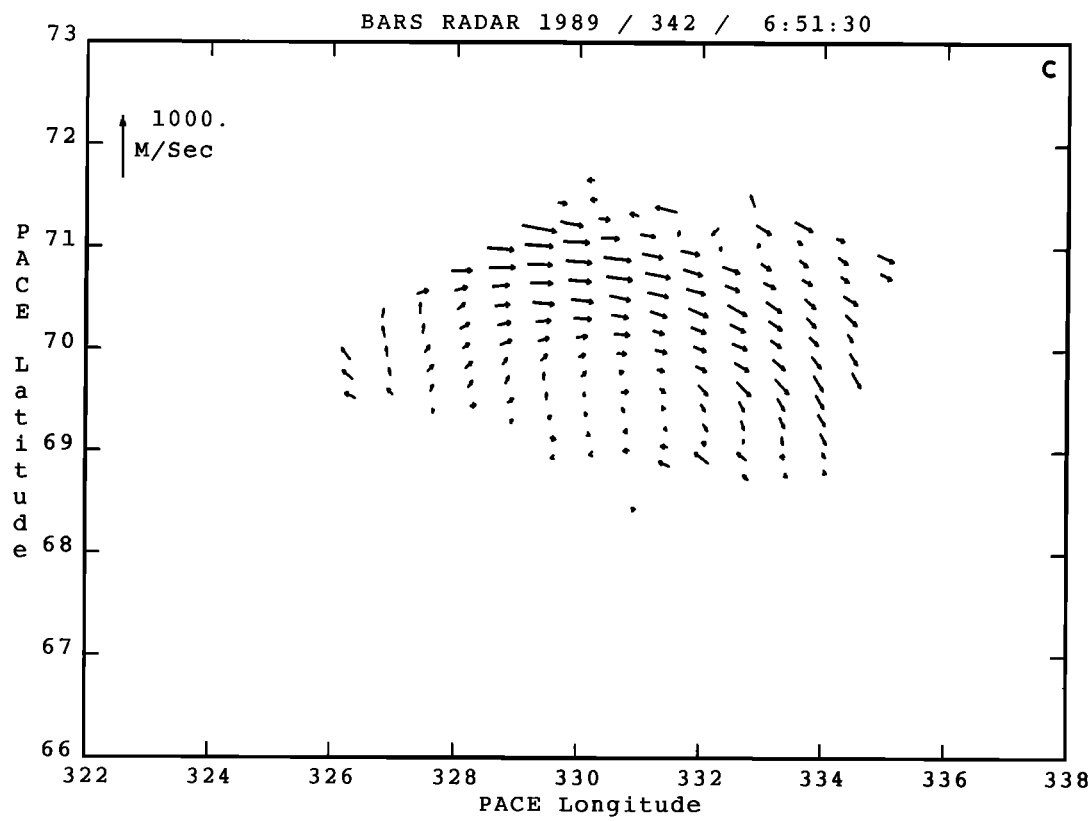

Fig. 2. (Continued)

In the present article, our primary objective is to determine whether FLRs with the observed velocity fields and azimuthal scale lengths might be nonlinearly unstable to the KHI in the equatorial plane of the magnetosphere. The formation of KH instabilities could play a role in dissipating the energy in FLRs and in the evolution of some of the vortex cells seen in the high-latitude electric fields, particularly the vortex structures seen during intervals with substorm intensifications [*Samson et al.*, 1992a]. There are other possible nonlinear effects which might play a role in the evolution of FLRs, including large FACs near the ionosphere, ponderomotive forces [*Allan et al.*, 1991], and the alpha-effect electromotive force [*Namikawa and Hamabata*, 1988]. These latter three nonlinear effects should not be present in our computational model.

In order to study nonlinear KHIs associated with FLRs, we have set up a computer simulation which uses a three-dimensional MHD code to follow the evolution and propagation of vorticity, from its source near the equatorial plane of the magnetosphere, to the region in the high-latitude ionosphere where it is observed. Our results indicate that the nonlinear KHI near the equatorial plane is likely the dominant mechanism leading to vortex structures in the resonances. We expect the instability to be localized to the equatorial plane for two reasons. First, the velocity shear is always a maximum there, and second, the wave magnetic field associated with the FLR is always a minimum in the equatorial plane. In the two directions perpendicular to the equatorial plane, the magnetic field of the Alfvén resonance will always have a stabilizing effect on the instability. We do not expect the KHI to grow near to the polar ionosphere. Instead, the vorticity generated by the instability in the equatorial plane will propagate to the ionosphere in the form of shear Alfvén waves. The FLRs we are interested in have wave periods of roughly a thousand seconds, and thus the propagation time to the ionosphere is of the order of a few hundred seconds. We shall show that the KHI evolves on a time scale significantly shorter than this, and consequently the ionosphere should play little role during the evolution of the instability.

A MODEL FOR NONLINEAR FIELD LINE RESONANCES

The nonlinear evolution of field line resonances can be investigated within the framework of the one fluid MHD equations described below,

$$\frac{\partial \rho}{\partial t} + \nabla \bullet \ (\rho \mathbf{v}) = 0 \tag{1}$$

$$\frac{\partial}{\partial t}\rho \mathbf{v} + \nabla \bullet \ (\rho \mathbf{v}\mathbf{v}) + \nabla \ P + \frac{1}{4\pi}\mathbf{B} \times (\nabla \times \ \mathbf{B}) = 0 \tag{2}$$

$$\frac{\partial \mathbf{B}}{\partial t} - \nabla \times \left[\mathbf{v} \times \mathbf{B} - \frac{\eta c^2}{4\pi}\nabla \times \ \mathbf{B}\right] = 0 \tag{3}$$

$$\frac{\partial}{\partial t}\rho E + P\nabla \bullet \ \mathbf{v} + \nabla \bullet \ (\rho E \mathbf{v}) + \eta J^2 = 0 \tag{4}$$

These equations describe conservation of mass ρ, momentum $\rho\mathbf{v}$, magnetic induction $\mathbf{B}$, and internal energy per unit mass E, respectively. Equation 4 can be rewritten in terms of P and $\mathbf{B}$ by using Ampere's law to eliminate the current density J, and the ideal gas equation of state,

$$\rho E = \frac{P}{\gamma - 1} \tag{5}$$

to eliminate the internal energy per unit mass in favor of the pressure P. The following evolution equation for the pressure then results,

$$\frac{\partial P}{\partial t} + \gamma \nabla \bullet \ (P\mathbf{v}) - (\gamma - 1)\left[\mathbf{v} \bullet \nabla \ P - \frac{c^2 \eta}{16\pi^2}(\nabla \times \ \mathbf{B})^2\right] = 0 \tag{6}$$

The system of equations (1)-(3), and (6) consist of eight nonlinear coupled partial differential equations for the unknowns ρ, $\rho\mathbf{v}$, $\mathbf{B}$, and P. They are solved numerically using techniques to be described below.

In order to gain an understanding of the structure of the FLR, as well as the starting point for the numerical solution of equations (1) through (6), we consider first of all the linearized form of the equations. Assuming that the plasma is inhomogeneous in the x direction, and that the ambient flow and resistivity are zero, we can derive from equations (1)-(6) the following vector wave equation for the perturbed velocity $\mathbf{u}$,

$$\begin{aligned}\rho_0 \frac{\partial^2 \mathbf{u}}{\partial t^2} &- \nabla(\gamma P_0 \nabla \bullet \ \mathbf{u} + \mathbf{u} \bullet \nabla \ P_0) \\ &+ \frac{1}{4\pi}(\nabla \times \ (\mathbf{u} \times \mathbf{B}_0)) \times \nabla \times \mathbf{B}_0 \\ &+ \frac{1}{4\pi}\mathbf{B}_0 \times \nabla \times (\nabla \times \ (\mathbf{u} \times \mathbf{B}_0)) = 0\end{aligned} \tag{7}$$

In deriving the above equation, pressure balance has been assumed in equation (2), and quantities with subscript zero refer to unperturbed values. Equation (7) can be solved assuming uniform magnetic field lines along z, with perfectly reflecting boundaries (i.e., conducting ionospheres) at $z = \pm L_z$. The boundary conditions at the ionospheres imply that the solutions will be composed of standing modes along z with wavenumber $k_z = m\pi/2L_z$, for $m = 0,1,2,...$,etc. The symmetry about the $z=0$ plane permits asymmetric and symmetric solutions. Since the difference between these solutions lies only in the location of the nodes and antinodes along z, we choose to consider the symmetric solutions, for which u_x has an antinode at $z=0$. The linearized version of equations (1), (3), and (6) imply that we can use a Fourier cosine series along z for ρ, p, u_x, u_y, and b_z, and a Fourier sine series for u_z, b_x, and b_y (for asymmetric modes the order would be reversed). Fourier transforming equation (7) in time and in the homogeneous spatial dimension y, and substitution of the appropriate Fourier series in z reduces the vector wave equation to a scalar equation in the Fourier amplitude u_x [*Chen and Hasegawa*, 1974],

$$\frac{d}{dx}\left[\frac{\rho_0 k_z^2 (v_p^2 - v_A^2)(c_s^2 + v_A^2)(v_p^2 - c_T^2)}{k_y^2 (c_s^2 + v_A^2)(v_p^2 - c_T^2) - k_z^2 (v_p^2 - v_A^2)(v_p^2 - c_s^2)}\frac{du_x}{dx}\right]$$

$$-\rho_0 k_z^2 (v_p^2 - v_A^2) u_x = 0 \tag{8}$$

where c_s and v_a are the sound speed and the Alfvén speed respectively, $v_p = \omega/k_z$ is the phase speed along z, and $c_T^2 = c_s^2 v_A^2/(c_s^2 + v_A^2)$. The y and z components of $\mathbf{u}$, and the magnetic field perturbations $\mathbf{b}$ are also expressible in terms of u_x:

$$u_y = \left[\frac{ik_y(c_s^2+v_A^2)(v_p^2-c_T^2)}{k_y^2(c_s^2+v_A^2)(v_p^2-c_T^2)-(v_p^2-v_A^2)(v_p^2-c_s^2)k_z^2}\right]\frac{du_x}{dx}$$

$$u_z = \left[\frac{-c_s^2(v_p^2-v_A^2)k_z}{k_y^2(c_s^2+v_A^2)(v_p^2-c_T^2)-(v_p^2-v_A^2)(v_p^2-c_s^2)k_z^2}\right]\frac{du_x}{dx} \quad (9)$$

$$b_x = -i\omega^{-1}k_z B_0 u_x$$

$$b_y = -i\omega^{-1}k_z B_0 u_y \quad (10)$$

$$b_z = i\omega^{-1}B_0\left[\frac{(v_p^2-v_A^2)(v_p^2-c_s^2)k_z^2}{k_y(c_s^2+v_A^2)(v_p^2-c_T^2)}\right]u_y - i\frac{u_x}{\omega}\frac{dB_0}{dx}$$

In the vicinity of the field line resonance at $x = x_0$ (where $\mathrm{Real}(\omega^2 - k_z^2 v_A^2(x_0)) = 0$, we approximate $(v_p^2 - v_A^2)$ as $-\frac{d}{dx}v_A^2(x_0)(x - x_0 + i\delta)$ and note that

$$\frac{ik_y(c_s^2+v_A^2)(v_p^2-c_T^2)}{k_y^2(c_s^2+v_A^2)(v_p^2-c_T^2)-(v_p^2-v_A^2)(v_p^2-c_s^2)k_z^2} \to \frac{1}{k_y^2} \quad (11)$$

and thus equation (8) reduces to

$$\frac{d}{dx}\left(\frac{x-x_0+i\delta}{k_y^2}\right)\frac{du_x}{dx} - (x-x_0+i\delta)u_x = 0 \quad (12)$$

Using the above expansions in equations (9)-(10), we find that in the vicinity of the FLR the velocity components in equation (9) behave as

$$u_{xR} \sim \ln(x-x_0+i\delta) + C$$

$$u_{yR} \sim \frac{1}{k_y}\frac{i}{x-x_0+i\delta}$$

$$u_{zR} \sim \left[\frac{c_s^2 k_z}{k_y^2(c_s^2+v_A^2)(v_A^2-c_T^2)}\frac{dv_A^2}{dx}\right]_{x=x_0} \quad (13)$$

and the magnetic perturbations in equation (10) behave as

$$b_{xR} \sim -i\omega^{-1}k_z B_0(\ln(x-x_0+i\delta)+C)$$

$$b_{yR} \sim \omega^{-1}B_0\frac{k_z}{k_y}\frac{1}{x-x_0+i\delta}$$

$$b_{zR} \sim \left[\frac{-\omega^{-1}B_0(v_A^2-c_s^2)k_z^2}{k_y^2(c_s^2+v_A^2)(v_A^2-c_T^2)}\frac{dv_A^2}{dx}\right]_{x=x_0} - i\frac{(\ln(x-x_0+i\delta)+C)}{\omega}\frac{dB_0}{dx} \quad (14)$$

where R subscripts refer to the shear Alfvén waves of the resonance, C is a constant independent of x, δ is a parameter defined by the expression,

$$\delta = \left(\frac{-2\omega_r\omega_i}{k_z^2\frac{d}{dx}(v_A^2)}\right)_{x=x_0} \quad (15)$$

and in equation (15) $\omega_r = k_z v_A$ and ω_i is a small parameter which has been introduced in order to remove the singularity which occurs at $x=x_0$ [*Chen and Hasegawa*, 1974; *Southwood*, 1974].

In Figure 3 we have plotted the real parts of equations (13) and (14) assuming $v_A^{-1}dv_A/dx = B_0^{-1}dB_0/dx = -0.8\,R_E^{-1}$ and $c_s/v_A = 2.25$. The parameter δ in equation (15) results in a finite width for the FLR and is chosen such that the spatial envelope of the velocity shear is of the order of 1 R_E. This is consistent with the results of *Mitchell et al.* [1990]. The parallel component b_z is relatively large (compared to b_x and b_y) for these parameters ($v_A > u_o$, where u_0 is the maximum shear velocity across the FLR), but remains a fraction of B_0. The finite compressibility of the plasma produces a nonzero component of velocity, u_z, along the field lines. However, near to the resonance $du_z/dx=0$, and it is expected that u_z will play only a minor role in the dynamics of any shear instability which develops from the FLR. We observe that in the vicinity of the resonance ($x = x_0$) there is a strong shear in both u_y and b_y. As a function of z, the velocity u_y, and the shear in u_y in the x direction, are maximized in the equatorial plane $z=0$. We also note that the corresponding solution for b_y vanishes at $z=0$ (recall that the solution for b_y is a Fourier sine series along z, while for u_y it is a cosine series). In the absence of a component of the wave magnetic field in the y direction, we expect the flows in the equatorial plane to be KH unstable. Out of the equatorial plane, b_y is nonzero and thus produces a stabilizing effect which is strongest at the ionospheres. The interaction between the regions of stability (towards the polar ionospheres) and the regions of instability (near to the equatorial plane) is the major focus of the present study.

In a three-dimensional configuration, FLRs can be unstable to the KHI and to current sheet or tearing mode (when finite electron inertia is included) instabilities. The nonlinear effects giving rise to each of these processes can be identified using the MHD equations (1)-(6). The convective nonlinear term $\nabla \cdot (\rho \mathbf{v}\mathbf{v})$ plays a role in the evolution of the KHI, whereas the nonlinear term $\nabla \times (\mathbf{v} \times \mathbf{B})$ plays a role in the formation of sheet current instabilities. In the linear analysis of the FLR we have assumed that the ambient flow velocity $v_o = 0$, and thus the nonlinear convection terms associated with the growth of the KHI, namely $\nabla \cdot (\rho \mathbf{v}\mathbf{v})$ in equation (2), have been eliminated through the process of linearization. We have, however, included the effect of a growing wave source by including a nonzero ω_i throughout the analysis, i.e., the term δ defined by equation (13) and used to obtain Figure 3. In equation (3), the nonlinear term $\nabla \times (\mathbf{v} \times \mathbf{B})$ can be expressed as $(\mathbf{B} \cdot \nabla\, \mathbf{v} - \mathbf{B}\nabla \cdot \mathbf{v} - \mathbf{v} \cdot \nabla\, \mathbf{B})$. When the field-aligned current and shear of the wave magnetic field are large, the last term in this identity can contribute to sausage and kink instabilities (this component is also not part of the linear analysis). In a magnetospheric context, the nature of the fundamental mode shear Alfvén standing wave implies that the convective nonlinear terms should be most important near to the equatorial region, and the current sheet nonlinear terms should be most important near to the ionosphere (non-

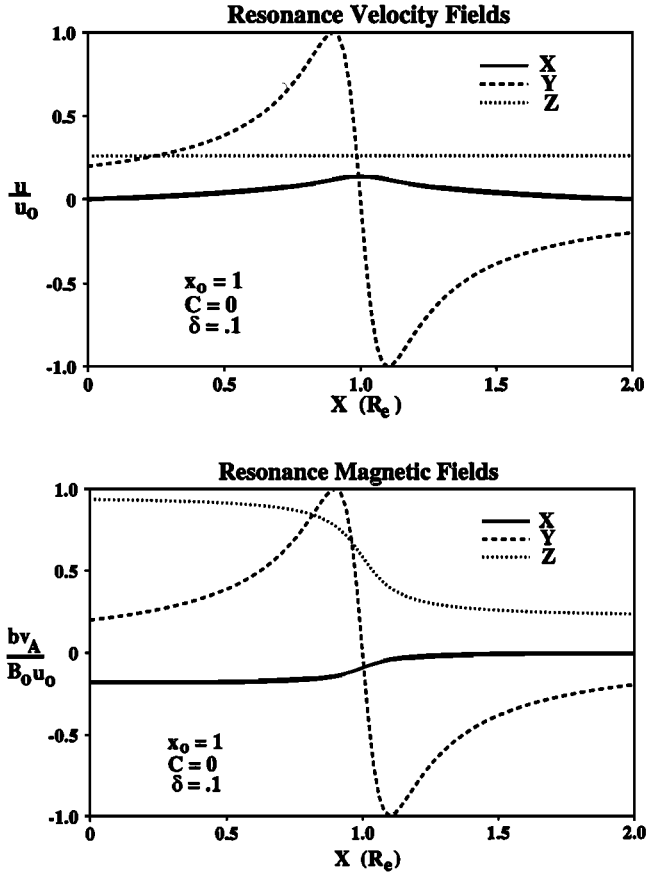

Fig. 3. Velocity profiles and magnetic field components corresponding to the FLR plotted as a function of radial position in the equatorial plane. The velocity and the magnetic field are out of phase by $\pi/2$ in time.

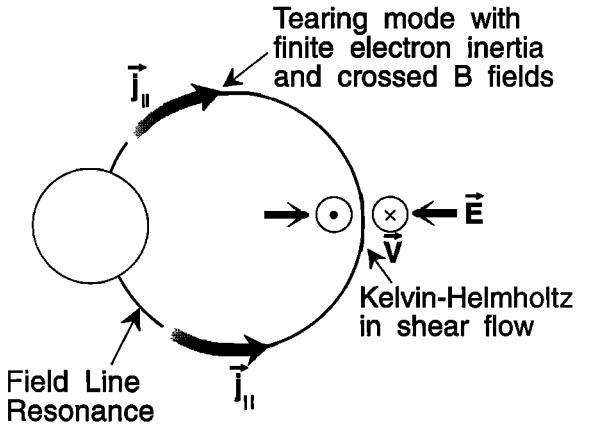

Fig. 4. A schematic of the FLR indicating positions where nonlinear processes are important. At the equator the nonlinearity is due to convection associated with the velocity field of the wave. At the ionosphere the dominant nonlinearity is due to the FAC and magnetic shear of the wave. The FLR is a standing wave with an electric and velocity field antinode at the equator and a corresponding wave magnetic field node.

ideal MHD effects such as collisionless tearing may be important here as well [*Seyler*, 1988]). These features are shown schematically in Figure 4. The numerical treatment of the full set of equations outlined in the next section includes the effects of both nonlinear terms. However, in the absence of a large resistivity at the ionosphere, this model, which uses a Cartesian geometry, produces currents within the resonances that are not large enough to cause nonlinear effects. In the actual magnetosphere, however, the geometry associated with dipole field lines is likely to lead to large FACs in the FLRs near to the ionosphere.

The formation of the KHI in the equatorial plane of a FLR should produce large-scale vortex structures which propagate to the ionosphere as shear Alfvén waves. In our computer models we will show that the growth times of the nonlinear KHI are significantly shorter than the Alfvén propagation time to the ionosphere and back. Consequently, "line tying effects" due to a conducting ionosphere are not important during the initial evolution of the KHI. In order to determine the feasibility of our KHI scenario, we can estimate the growth rates and scale sizes of the instability by using the measured velocity fields in the ionosphere [*Samson et al.*, 1992a] and mapping these fields to the equator. We can then use these velocity fields, and the growth rates computed using linearized MHD equations, to make a rough estimate of the growth rate [*Hollweg and Yang*, 1988] for the KHI associated with the FLR. The KHI has a maximum growth rate at an azimuthal wavenumber k_y given by $k_y\Delta \sim 0.6$, where 2Δ is the radial thickness of the velocity shear associated with the FLR in the equatorial plane of the magnetosphere [*Walker*, 1981]. The measured values of the latitudinal widths of the FLRs in the ionosphere are often 40 km or less [*Samson et al.*, 1992a; *Walker et al.*, 1992], and the region of velocity shear might be of the order of 20 km. Using these values, we estimate that the azimuthal wavelength of the KHI should be approximately 15-20^0. The maximum growth rate of the KHI occurs at a wavelength that is roughly 10 times the thickness of the FLR, and consequently we can make a rough estimate of the growth rate using the expression for a discontinuous change in velocity, namely,

$$\omega_i^2 = \frac{\rho_1\rho_2}{(\rho_1+\rho_2)^2}[\mathbf{k}\cdot(\mathbf{v}_2-\mathbf{v}_1)]^2 - \frac{(\mathbf{B}_1\cdot\mathbf{k})^2+(\mathbf{B}_2\cdot\mathbf{k})^2}{4\pi(\rho_1+\rho_2)} \quad (16)$$

where ρ is the density, and v is the fluid velocity. In the present case, subscript 1 indicates the earthward side of the resonance, and subscript 2 indicates the antiearthward side. The maximum growth rate occurs for **k** perpendicular to **B** and parallel or antiparallel to **v**, or in the azimuthal direction in the equatorial plane. Since the perpendicular magnetic field of the FLR is zero at the equatorial plane (z=0), then $B_1 = B_2 \sim B_0$, and assuming that ambient convection is small we have $\mathbf{v}_1 = -\mathbf{v}_2$. Assuming also that there is little change in density across the resonance gives the following expression for the growth rate: $\omega_i^2 = k_y^2v^2 - k_z^2v_A^2$, where $v = |v_1| = |v_2|$. In the ionosphere, the resonances have a velocity of 1km/s or so and a conservative mapping to the equatorial plane gives a flow velocity exceeding 80 km/s. At the estimated position of the resonances (on the magnetic shell L=9), our previous estimate for the azimuthal wavenumber k_y~m/r, with m=360^0/20^0/λ=18 and r=9 R_E, corresponds to an equivalent k_y of approximately 2 R_E^{-1}. The length corresponding to L=9 dipole field lines is 22.8 R_E, which implies that the fundamental mode should have a k_z of approximately $0.14R_E^{-1}$. At an Alfvén speed of 1000 km/s, for example, the threshold for instability in this region should therefore occur at a velocity v~70 km/s. Assuming that the flow velocity is 80 km/s gives a growth rate $\omega_i^{-1} \sim 80$ s. Note that in the warm central plasma sheet, the threshold for instability is expected to be considerably lower than our estimate above, due to compressibility effects (see, for example,

Figure 2 of *Walker* [1981]). Although the above calculations are approximate, the important point here is that the estimated growth times are much less than the observed periods of the resonances (typically 500-1000 s) [*Samson et al.*, 1992a].

COMPUTATIONAL MODEL AND INITIALIZATION

We have investigated the nonlinear evolution of a model field line resonance using a Cartesian, fully three-dimensional resistive magnetohydrodynamic computer simulation code. A three-dimensional code, describing variations in the radial, azimuthal and field-aligned directions, is necessary since nonlinear effects require azimuthal variation. We shall describe the model in detail, since it is our intention to use it as a platform for future investigative studies of MHD processes in the Earth's magnetosphere. First of all, we describe the basic equations which are solved and summarize the numerical methods, boundary conditions and initialization which are used in the investigation of the model problem to be discussed below. As mentioned above, for the class of problems we shall be concerned with, the nonlinear terms in the equations must be retained, and so we adopt a numerical approach in our search for solutions.

We solve the nonlinear equations using a Newton Raphson iteration scheme and a time splitting algorithm called the Douglas-Gunn alternating direction implicit (ADI) method [*Douglas and Gunn*, 1964]. Equations (1)-(3) and (6) are first expressed in finite difference form on a three-dimensional Cartesian grid. Given initial conditions at time t=0, the algorithm proceeds by advancing the unknowns implicitly from time level n to time level n+1. The implicit time advancement means that large (i.e., exceeding the Courant limit) time steps can be taken, since all points on the grid are synchronized in time. This can be particularly important when large gradients in the Alfvén velocity are present, or when resistive time scales are to be resolved. The ADI method is second-order accurate in both space and time and accomplishes its overall time advancement in three basic steps. The first step advances the solution in time with respect to the x coordinate direction only. That is to say, the advanced time level is assigned only to those derivative terms which contain x as their dependent variable. After the solution in the x direction has been completed, the state vector $\mathbf{U}=[\mathbf{B}, \rho, \mathbf{v}, P]$ is advanced in time with respect to the y direction, and finally with respect to the z direction. The advantage of this approach is that the solution method proceeds as a series of one-dimensional updates to the state vector $\mathbf{U}$, and thus places modest demands on computer memory resources and cpu time. One complication arises due to the presence of mixed derivative terms in the equations. These terms, caused by the plasma resistivity, couple adjacent coordinate sweep directions on the mesh. We deal with this problem by treating these terms explicitly, i.e., they are assigned time level n. This sets a Courant condition for the mixed derivative terms, but this is not normally of significance, and does not limit the algorithm severely. The reader is referred to the articles by *Briley and MacDonald* [1977], and by *Finan and Killeen* [1981] for the relevant details.

From a computational point of view, it is worth pointing out that the ADI method, as described above, multitasks very well. We have implemented the algorithm on a four-processor Stardent 3040 computer, and on a Myrias SPS-3 computer (44 processors), and have obtained near perfect parallelism. One disadvantage of the implicit method is that block tridiagonal systems of equations must be solved for each sweep direction on the mesh. This is the most time-consuming part of the calculation, since the standard Gaussian elimination method of solution does not easily vectorize or parallelize. This is a standard problem in numerical work, and there is currently much interest in finding algorithms which make efficient use of modern computer architectures. One such approach is block cyclic reduction, as outlined in the paper by *Anderson et al.* [1987]. We hope to investigate this and other methods in the future.

Our computational grid uses a Cartesian geometry, with x representing the radial direction, y the azimuthal direction, and z the direction of the geomagnetic field. The system is periodic in the y direction and has reflecting boundaries in the x direction. The system is approximately 2 R_E in width in the x direction and 1 R_E in width in the y direction (corresponding to the anticipated wavelength for maximum growth of the KHI). We consider the ionospheres to be perfect conductors and use boundary conditions appropriate to a standing Alfvén wave. Specifically, the boundary conditions are that the tangential electric field and the normal velocity component should vanish. Although in reality the ionosphere is not a perfect conductor, and in fact can have substantial gradients in conductivity, these effects are not important during the relatively long time interval over which vorticity is expected to propagate from the equatorial plane to the polar ionosphere. Of course, they will become important after the vorticity reflects off of the ionosphere. We leave this more difficult situation open for future study.

While the velocity shear in the solution of the linear equations (8)-(10) is a consequence of the inhomogeneous Alfvén velocity profile, the subsequent nonlinear development of the shear instability is not expected to be critically dependent on the nonuniformity of the system. This is because the KHI arises in systems of uniform and nonuniform densities (and/or magnetic fields). Thus once the shear has been established, the instability can grow regardless of nonuniformities. For the sake of simplicity, we therefore take as our starting point a finite amplitude Alfvén wave with the structure of an Alfvén resonance in a uniform system. This choice considerably simplifies the analysis of the three-dimensional data sets generated by the MHD code, and in particular it requires substantially less cpu time. We have simulated the two-dimensional KHI at the equatorial plane including the effect of nonuniformities and have obtained qualitatively very similar results. Specifically, we initialize the computational model with uniform ambient plasma density and magnetic fields, through which propagates (1) a shear Alfvén wave with a specified wave period and (2) a significantly smaller amplitude shorter scale length transverse velocity perturbation which acts as a seed for the KHI. The scale lengths and amplitudes of the Alfvén wave and the perturbation are selected so as to be consistent with the FLR structure shown in Figure 3. The ambient plasma conditions correspond to $\mathbf{B}_0 = B_0 \mathbf{e}_z$, with $B_0 = 4 \times 10^{-4}$ G, v_A=280 km/s, and T_0=2 keV, where B_0 represents the geomagnetic field, v_A is the average Alfvén velocity, and T_0 is the average plasma temperature, respectively. The shear Alfvén waves propagate between perfect conducting ionospheres at $z = \pm\pi/2k_z$, where k_z is the z component wavenumber corresponding to the Alfvén wave resonance.

The shear Alfvén wave resonance magnetic field may be expressed as $\mathbf{b}=b_{xR}\mathbf{e}_x+b_{yR}\mathbf{e}_y$, with corresponding velocity components v_{xR} and v_{yR}. The length scale and amplitude of the Alfvén wave velocity shear in the equatorial plane of the magnetosphere are based on the experimentally obtained data, as explained in the discussion leading to Figure 3. The velocity shears in the ionosphere are typically 1 km/s in a 20- to 50-km latitudinal interval. Mapping these estimates to the equatorial plane indicates that velocity jumps of 200 km/s across the FLR should be possible. As mentioned above, we add a transverse velocity perturbation (of amplitude ε) to seed the KHI. This perturbation has a Gaussian spatial dependence in the x direction and is localized within the velocity shear region. The initial spatial profiles of $\mathbf{v}$ and $\mathbf{B}$, corresponding to the shear Alfvén wave and the perturbation, are indicated below

$$v_x = v_0 e^{-x^2/\Delta^2} [\cos(k_z z)\cos(k_{yR} y) + \varepsilon \cos(k_z z)\cos(k_y y)] \quad (17)$$

$$v_y = -\frac{v_0}{\Delta k_{yR}} \frac{2x}{\Delta} e^{-x^2/\Delta^2} \cos(k_z z)\sin(k_{yR} y) \quad (18)$$

$$b_{xR} = -B_0 \frac{v_0}{v_A} e^{-x^2/\Delta^2} \sin(k_z z)\cos(k_{yR} y) \quad (19)$$

$$b_{yR} = -B_0 \frac{v_0}{v_A} \frac{2x}{\Delta} \frac{1}{\Delta k_{yR}} e^{-x^2/\Delta^2} \sin(k_z z)\sin(k_{yR} y) \quad (20)$$

In the above expressions, the z coordinate is measured with respect to the equatorial plane, v_A is the Alfvén velocity, v_0 is the peak flow velocity in the y direction associated with the model FLR, 2Δ is the localization width of the resonance, and all quantities have an assumed harmonic time dependence. The analytic profiles above (in basic agreement with the relevant parameters of Figure 3) are consistent with a standing shear Alfvén wave with a node in b_{yR} at the equator, and antinodes in v_{yR} and v_{xR}, respectively. Note that in the above expressions the k_{yR} and k_y dependences are associated with shear Alfvén waves and KHI excited waves, respectively. We assume that small-scale turbulence (with $k_y >> k_{yR}$) in the plasma sheet seeds the instability, so that the variation with respect to k_{yR} does not play a strong role in the evolution of the dynamics and can therefore be neglected (this is in agreement with the observations). However, the approximate $\pi/2$ phase difference between v_{xR} and v_{yR} indicates that different longitudinal positions y will be more or less unstable. We choose a longitudinal position for which v_{yR} is a maximum. This position corresponds to a maximum in the growth rate for the instability. A normal mode analysis of the two-dimensional problem ($k_z = 0$), with a hyperbolic tangent region of velocity shear, indicates that the most unstable wavenumber of the KHI occurs for $k_y \sim 0.6/\Delta$ [*Walker*, 1981]. However, for the FLR problem a normal mode analysis of the linear equations (computed numerically) shows that the additional shear zones push the maximum growth rates to higher wavenumbers: $k_y \sim 1.2/\Delta >> k_{yR}$. The three-dimensional instability must also satisfy $\omega_i >> \omega_R$ (where ω_i is the growth rate of the instability and ω_R is the frequency of the shear Alfvén wave) for there to be appreciable growth of the instability before the Alfvén fields change sign. Shorter scale perturbations would not have time to grow within the time period of the oscillating Alfvén wave field. The above choice for k_y then determines the periodicity length of the computational grid in the y direction. We also set the resistivity term η to a small value since it is not important for the evolution of the KHI at the equatorial plane, and in fact is not known in practice. The value selected ensures that our numerical scheme is stable to numerical noise.

In summary form, the wave parameters corresponding to the FLR are as follows: k_{yR}=0.3 R_E^{-1}, k_y=6.8 R_E^{-1}, k_z=0.1 R_E^{-1}, v_A=280 km/s, $\sqrt{2}v_0/e^{1/2}k_{yR}\Delta$ = 90 km/s Δ = 0.18R_E, ε = 0.02, shear Alfvén wave period τ = 1380 s; satisfying $k_y >> k_{yR}$ and $k_{yR}y$->constant (π/2). The latter approximation implies that the v_x velocity component is then entirely due to the KHI. Note that we have used a longer wave time period (smaller value of v_A) than is typically observed (1000 s) in order to identify clearly effects associated with the propagation of the instability to the ionosphere. There is evidence in the data presented by *Mitchell et al.* [1990] that the oscillation period of waves in FLRs at 10.5 R_E are consistent with higher particle densities (smaller v_A) than might be anticipated (1 per centimeter cubed). However, our choice of wave period is principally a matter of convenience.

The velocity profiles in the equatorial plane, sketched as a function of the x coordinate in Figure 3, clearly show the three regions of velocity shear across the FLR. The largest jump in velocity occurs across the center of the FLR, and it is this region that will be the most unstable to the KHI. In order to determine the characteristic growth time for the instability at the equatorial plane, it is first of all worthwhile considering the following two-dimensional simulation. Consider the situation in which the oscillating Alfvén wave velocity component v_{yR} has reached its peak value. Suppose also that the period of the wave is effectively infinite, and that variations with respect to the geomagnetic field direction are negligible. The KHI, with initial conditions defined by equations (17)-(20), is effectively an instability in the v_x component of velocity. In Figure 5 we show the growth in the maximum value of v_x as a function of time. Figure 6 is a log linear fit to the data displayed in Figure 5 for the time interval over which exponential growth is taking place. The

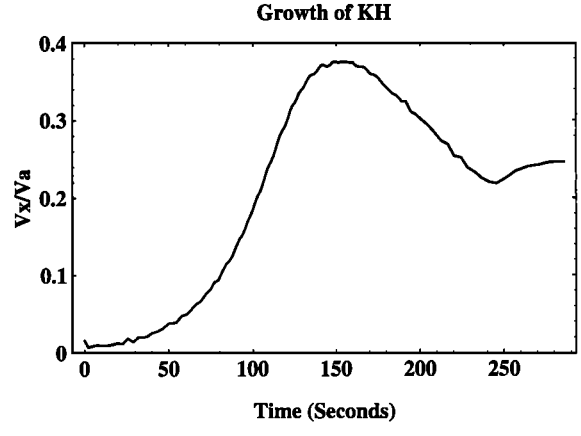

Fig. 5. Growth of v_x component of velocity, corresponding to the KHI in the equatorial plane. The period of the shear Alfvén standing wave is effectively infinite, and propagation effects are neglected.

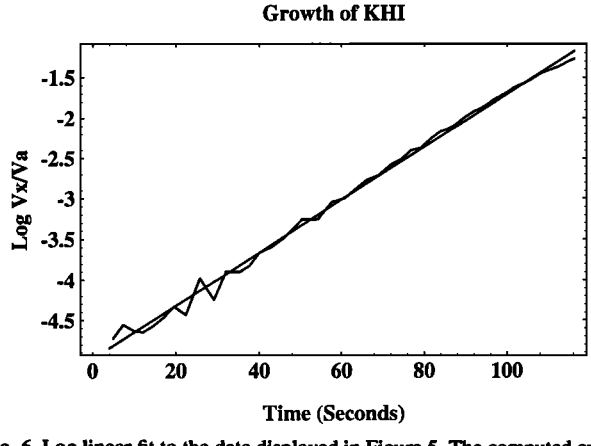

Fig. 6. Log linear fit to the data displayed in Figure 5. The computed exponential growth rate is 0.0333 s^{-1}.

computed growth rate is approximately 0.0333 s^{-1}, corresponding to an exponentiation time interval of 30 s. It can be seen that the instability saturates at t=150 s, following which it is observed to decay and eventually settle into a series of quasi-steady oscillations with an amplitude of roughly 60 percent of the saturation value. Saturation occurs because the flow contains a finite amount of vorticity initially. The small-scale oscillations on the curve in Figure 5 are caused by compressional Alfvén waves, which bounce back and forth across the numerical grid in the x direction. These waves, which are a by-product of the initialization (the velocity field perturbation is not divergence free initially), are always of small amplitude and do not play a role in the evolution of the instability. The above results should be kept in mind when considering the three-dimensional simulations to be described below.

The three-dimensional simulations produce large quantities of data from which only representative results can be shown. As indicated above, the principal velocity shears are in the x-y plane, and therefore we shall examine cuts of the data in this plane. All times will be referenced from t=0, which corresponds to the phase of the shear Alfvén wave for which $v_{yR}(x,y,z,t=0)=0$. Note that the wire frame graphics at our disposal require uniformly spaced data values. Therefore the results are displayed as interpolated values, reflecting the fact that the numerical grid is nonuniform in the x direction. In reality the grid has approximately twice as many data points across the resonance width than the figures indicate. In all cases the simulation grid spans 2 R_E in the x direction, and 1 R_E in the y direction. In order to make the plots more visible the grid is clipped by 0.4 R_E at the maximum and minimum x values, respectively, so that the center of the velocity shear is at x=0.6 R_E with respect to the origin.

The velocity field in the x-y plane at the equator, showing the time development of vortices produced by the KHI, is displayed in Figure 7. Figure 7*a* shows the velocity shears present at t=50 s, corresponding to the growing shear Alfvén wave field of the FLR. Figure 7*b* shows the KHI which has developed by t=217 s. A large-scale vortex is in the process of forming in the top half of the figure, whereas two smaller scale vortices are evolving on either side of the FLR in the lower half of the figure. The smaller scale structures are caused by the velocity jumps across the two outside edges of the resonance, which are themselves unstable to the KHI. These small-scale vortices produce interesting flow patterns during the temporal development of the instability, but do not seem to affect the overall dynamics appreciably. Figure 7*c* shows the instability later in time at t=248 s. At this stage in the dynamics, the instability is well into the nonlinear regime even though the peak flow velocities in the FLR have not yet been reached. Figure 7 also shows clearly the spatial distortion of the FLR that is produced by the KHI. The instability grows most rapidly inside the center portion of the resonance (since the largest velocity jumps occur there), and the rotational motion that subsequently develops is restricted by the relatively undisturbed parallel (i.e., vertical in Figure 7) flows on the velocity shear regions on the outside of the FLR. The net effect of this is to distort straight stream lines on the outside of the FLR into S-shaped streamlines, the eccentricity of which grows with time. By the time indicated in Figure 7*c*, the distortion of the FLR is rather severe. The small-scale vortices in Figures 7*b*,*c* are corotating and can lead to the formation of very sharp velocity shears in the region where they are strongly interacting, particularly at the nonlinear stage. In our simulations there is some indication that a cascade of these small-scale vortices to shorter wavelengths may result. However, our numerical grid was not sufficiently resolved to investigate this effect in detail.

The centripetal forces associated with the KHI rotational motion

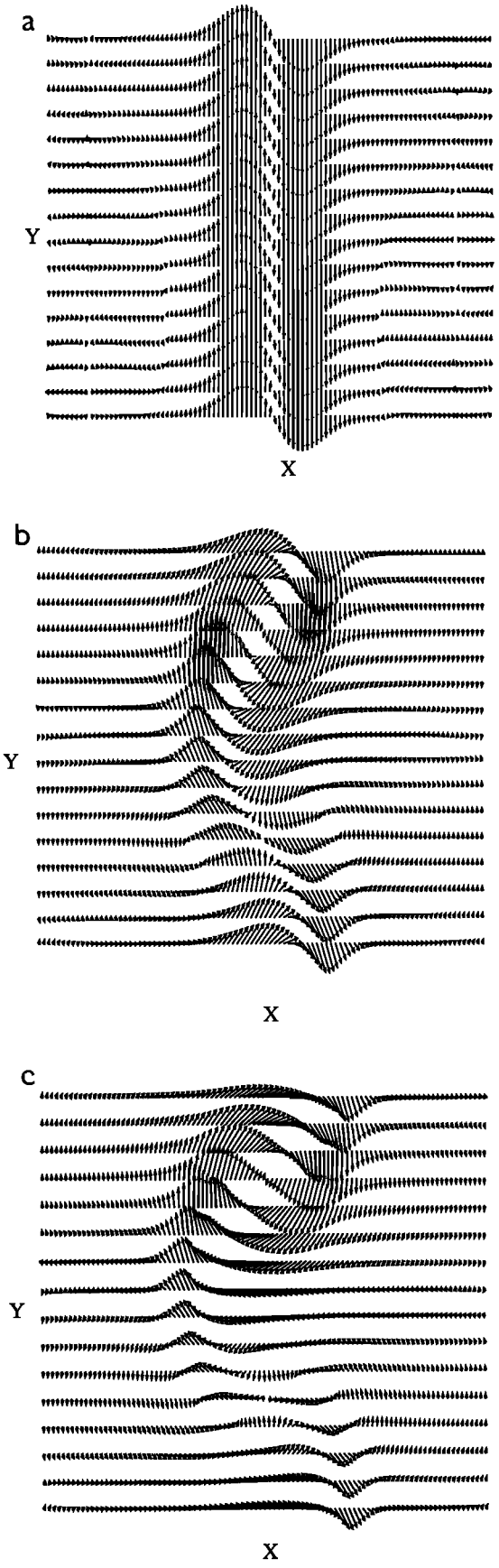

Fig. 7. Velocity field in the x-y plane at the equator, showing the evolution of the KHI. The center of the FLR is situated at 8-10 R_E in the equatorial plane. The X coordinate spans 2 R_E and the Y coordinate spans 1 R_E: (a) t=50 s, (b) t=217 s, (c) t=248 s.

of the plasma act to produce a density minimum at the center of the FLR. Since the plasma is "frozen-in," the ambient magnetic field is carried with the motion and also develops into a local minimum. However, the perturbations in the density and in the ambient magnetic field B_0, are not noticeable until the nonlinear stage of evolution has been reached. For example, the magnetic perturbation b_z in Figure 8*a* has not evolved significantly beyond the ambient conditions in spite of the fact that vortices are well formed by this time, i.e., t=200 s. Figure 8*b* shows the magnetic perturbation later in time, t=300 s, at a stage where the instability is nonlinear (the peak in Figure 8*b* is inverted and corresponds to a decrease in the magnetic field). The actual fluctuation in the z component of the field is still small and amounts to approximately 2.5 percent of the ambient magnetic field. There are no field-aligned currents produced in this case since we are examining the equatorial plane where b_{yR} is zero.

The circulation patterns associated with the KHI, and its distortion of the FLR, are clearly visible in the z component of the vorticity function, which we define here as $\mathbf{e}_z \cdot (\nabla \times \mathbf{v})$. This is now the preferred form for presentation of the data, particularly since J_z is proportional to the curl of **B**, and has a topologically similar form. For example, in Figure 9 we show the development of vorticity in the equatorial plane as a function of time. Figure 9*a* shows the vorticity in the x-y plane at the equator at time t=105 s just as the instability is starting to form. Figure 9*b* shows the vorticity at the equator later in time, at t=172 s, and in Figure 9*c*, the instability is displayed at a stage, t=217 s, where a closed circulation flow has developed. The characteristic "wrapping up" of the vorticity is clearly present at this stage, and is more apparent in Figure 9*d*, which shows the vorticity at time t=248 s. The sharp ridges in the latter figure are more defined and are separating due to broadening of the instability in the direction transverse to the ambient flow. These "ridges" mark points of inflection in the velocity field, and serve to highlight the distortion of the resonance by the KHI. In viewing the above results, it should be remembered that the system is periodic in the y direction. Thus when the flow encounters the system boundary at the y=0 face of the enclosing box in Figure 9*d*, it is mapped to the opposite face at $y=y_{max}$ and therefore the results correspond to a train of vortices being produced in the equatorial plane of the actual magnetosphere. At the stage in the dynamics indicated in Figure 9*d*, the instability is almost saturated spatially, i.e., it does not broaden very significantly with respect to x in the equatorial plane after this time (its transverse extent stays more or less confined to the original scale size of the resonance). However, the shear Alfvén wave is still cycling towards the peak velocity that it can attain during an oscillation period, namely its value at t=350 s. The instability continues to be modulated in time over a half wave period due to the basic harmonic frequency dependence of the shear Alfvén wave. At the time shown in Figure 9*d*, the instability is essentially localized to the equatorial plane. For example, the ambient vorticity is not affected in the z plane situated approximately one quarter of the distance from the equator to the ionosphere. The instability has not yet reached this part of the magnetosphere because propagation effects have not had time to occur.

As remarked earlier, the v_x component of velocity acts as a signature for the KHI. We show in Figure 10 the growth of the maximum value of v_x in the equatorial plane as a function of time. The points marked a, b, c, and d correspond to the times indicated in Figure 9, and the evolution is shown over a time interval in excess of the half wave period of the shear Alfvén waves, i.e., 900 s. It is clear that the instability is saturated spatially on a time scale which is significantly shorter than the period of the FLR. The computed growth time for e folding the amplitude by a factor of 10 is found to be approximately 200 s. If we assume that the average growth time for the instability scales linearly with v_0, then the timescale for a tenfold increase lengthens to 600 s for a flow velocity of 30 km/s at the equator. However, it is almost certainly true in the magnetosphere that the levels of noise present exceed the 2 percent values that are used here. More likely, the source of noise is broadband and typically at a level approaching 10 percent during active periods. It may not require a significant exponentiation of the disturbances in order to produce vortex structures at the equator. We have also simulated model FLRs having a peak flow velocity less than is necessary for growth of the KHI within a half wave period. We find that under these circumstances the oscillations of the FLR destroy the

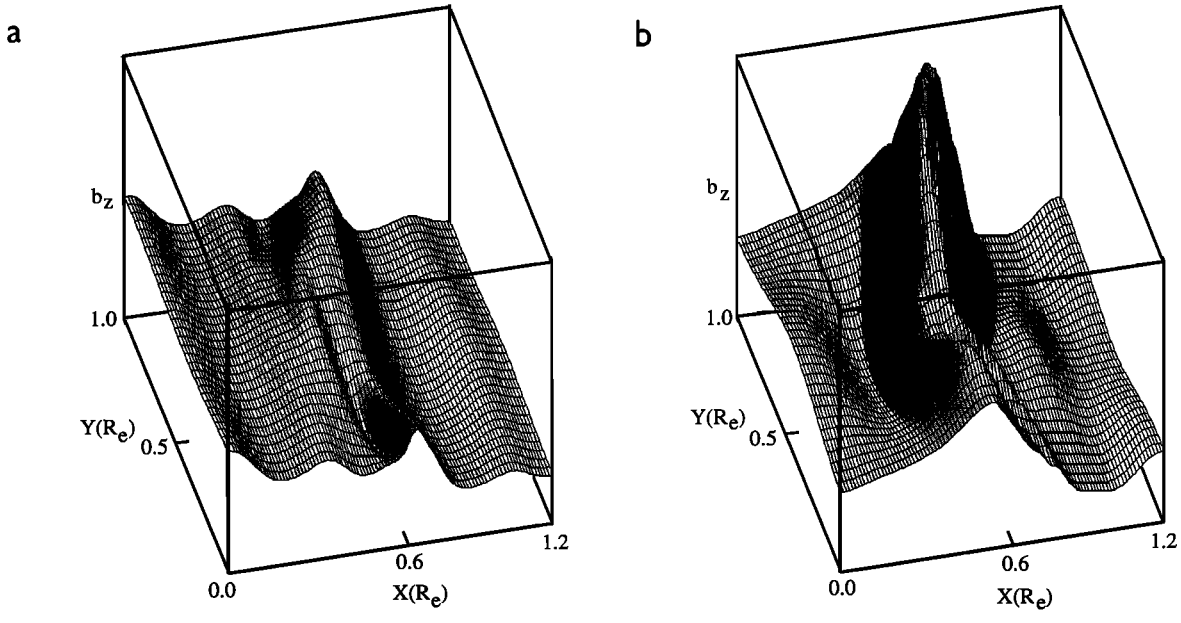

Fig. 8. Magnetic perturbation b_z (in arbitrary units) associated with the KHI in the equatorial plane: (a) t=200 s, (b) t=300 s. The peak in Figure 8b corresponds to a magnetic field minimum. The maximum fluctuation is approximately 2.5 percent of B_0. The X coordinate simulation grid is 2 R_E across and has been cropped to emphasize the FLR.

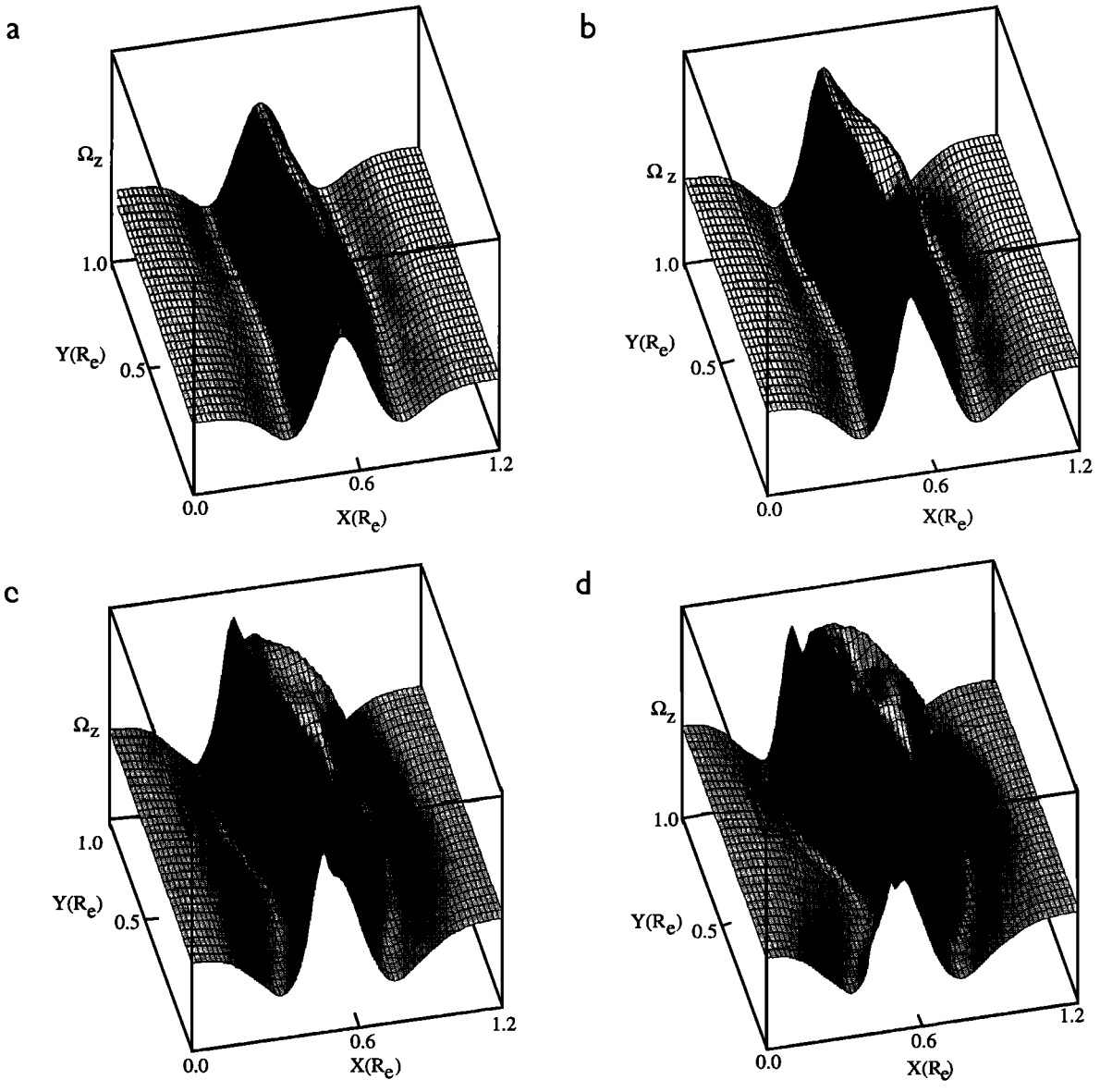

Fig. 9. Vorticity Ω_z (in arbitrary units) associated with the three-dimensional KHI in the equatorial plane. The center of the FLR is situated at 8-10 R_E in the equatorial plane. Times are referenced from the point during the cycle of the shear Alfvén standing wave for which v_{yR}=0: (a) t=105 s, (b) t=172 s, (c) t=217 s, and (d) t=248 s.

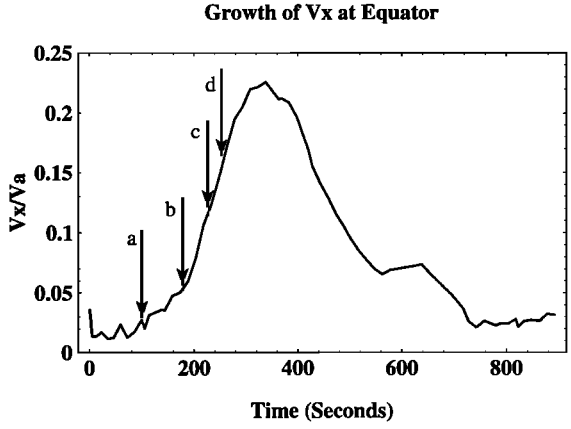

Fig. 10. Growth of the v_x component of the three-dimensional KHI in the equatorial plane. The time interval on the curve corresponds to a half wave period of the shear Alfvén standing wave.

conditions for growth, i.e., there is no time-averaged growth of the instability. Figure 11 shows the growth of the x component of velocity near to the ionosphere. In viewing this figure, it should be noted that vortex structures from a KHI at the equator would not be expected to reach the ionosphere until a quarter wave period after the onset of the instability. In the simulations, we observe significant increases in v_x at the equator at a time between t=50 s and t=75 s . Propagation effects would then produce vorticity at the ionosphere at a time between t=400 s and t=425 s. This coincides with the sharp increase in v_x which can be seen in Figure 11. Note also in Figure 11 that noise is present in v_x until propagation effects have had time to occur.

The increase in v_x near to the ionosphere does not by itself imply that vorticity is present. Figure 12 shows the vorticity which develops near to the ionosphere after propagation effects have had time to occur. In Figure 12*a*, the vorticity at t=400 s coincides with the arrival of shear Alfvén waves from the equatorial plane. It should

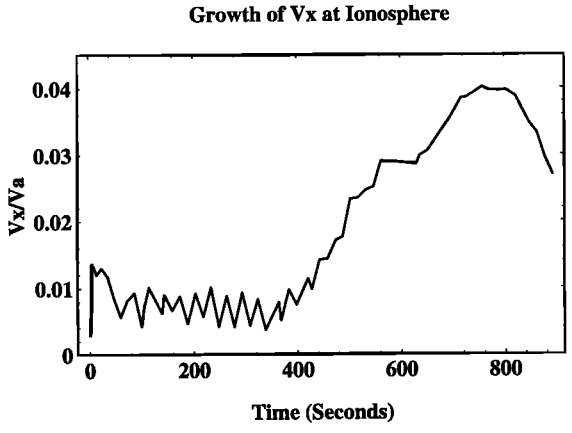

Fig. 11. Growth of the v_x component of the three-dimensional KHI near to the ionosphere.

be remembered that close to the ionosphere the FLR has a velocity node, so that the ambient vorticity present in Figure 12 is small. The vorticity present at t=475 s, and at t=600 s is shown in Figures 12*b* and 12*c*, respectively. The wrapping up of the vorticity is now visible but is spatially more broad than in Figure 9, in accordance with the fact that before propagation effects can occur at the equator, the instability there is very nonlinear and consequently is also spatially broadened. It should also be remembered that the magnetic field b_{yR} associated with the FLR is zero at the equator and is a maximum at the ionosphere. Furthermore, b_{yR} and v_{yR} are out of phase by $\pi/2$ in time. Thus in the time it takes vorticity to propagate from the equatorial plane to the ionosphere, the magnetic field of the shear Alfvén wave has decreased from its maximum value, changed sign, and is cycling towards its minimum value. This can lead to some rather complicated flow patterns during the temporal evolution of the vorticity at the ionosphere. However, we can still identify characteristic features associated with the KHI. For example, the magnetic fluctuation b_z which develops near to the ionosphere at times coincident with those in Figures 12*a* and 12*c*, is plotted in Figure 13. Figures 13*a* and 13*b* indicate that there is no significant component of b_z before propagation effects have had time to occur. Furthermore, since perturbations in b_z are generally only visible during the nonlinear stages of the instability, it can be inferred, from the topological similarity between Figure 13*b* and Figure 8*b*, that the nonlinear KH disturbances produced at the equatorial plane are readily mapped along the geomagnetic field lines to the ionospheric plane.

The propagation effects associated with the KHI at the equatorial plane also modify strongly the field-aligned currents associated with the FLR (at all spatial positions along geomagnetic field lines in the vicinity of the FLR). The maximum modulus of the field aligned current density in the z plane near to the ionosphere is plotted as a function of time in Figure 14. A maximum in the current density occurs at the ionosphere due to the antinode in b_{yR}. In Figure 14 the current density is significantly reduced during the second quarter cycle of the shear Alfvén wave due to nonlinear effects associated with the propagation of the instability to the ionosphere. This can also be seen in Figure 15, which shows a time sequence of the evolution of the field-aligned current density in the x-y plane near to the ionosphere. In the absence of the instability, J_z consists of current sheets (extending along the geomagnetic field lines) corresponding to the magnetic shear in b_{yR} associated with the FLR. As shown in Figure 15, the vorticity associated with the propagation of the instability from the equatorial plane to the ionosphere distorts

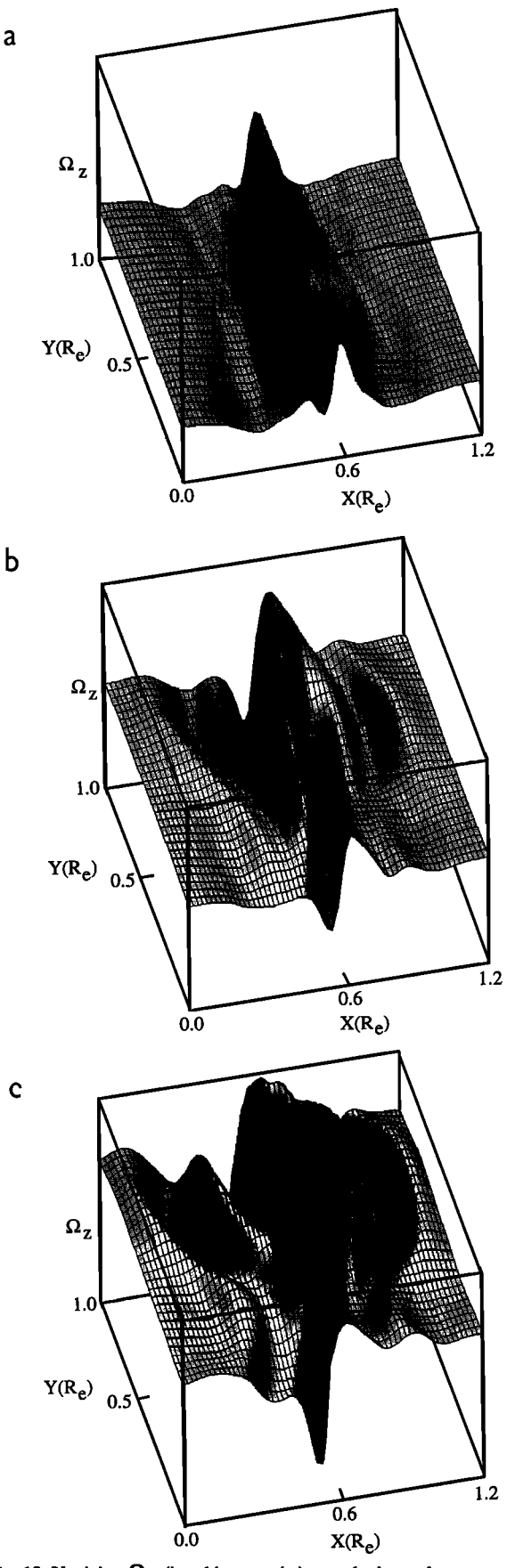

Fig. 12. Vorticity Ω_z (in arbitrary units) near the ionosphere, corresponding to propagation effects associated with the three-dimensional KHI at the equatorial plane. The center of the FLR is situated at 8-10 R_E in the equatorial plane: (a) t=400 s, (b) t=475 s, and (c) t=600 s.

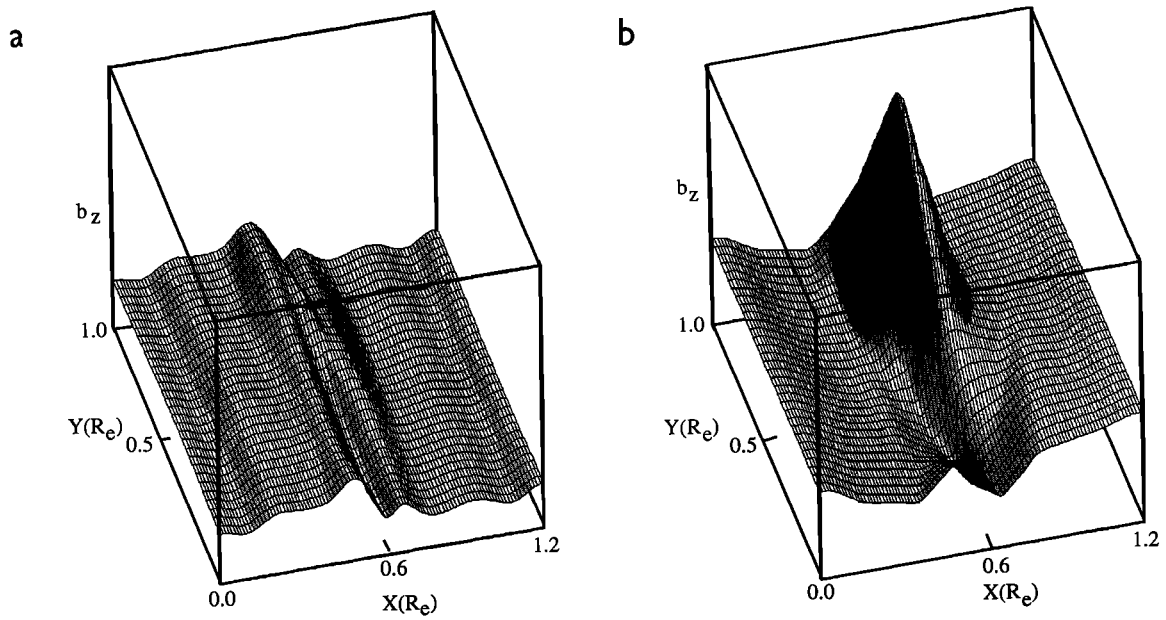

Fig. 13. Magnetic perturbation b_z (in arbitrary units) associated with the propagation of vorticity from the equatorial plane to the ionosphere: (a) t=400 s and (b) t=600 s.The maximum fluctuation is approximately 2.0 percent of B_0.

the current sheets appreciably. In particular, the instability spreads and wraps up the current sheets in the transverse direction and reduces their amplitude significantly. Again, this is true not only at the ionosphere, but also along the entire length of the geomagnetic field lines. The overall situation is therefore one in which a strong localized source of vorticity develops at the equatorial plane and propagates with time towards the ionosphere, in the process of which it severely distorts the magnetic fields of the resonance. From the evidence in Figures 14-15, it is clear that the KHI at the equatorial plane eventually leads to a significant decay and dissipation of the FLR within a fraction of a shear Alfvén wave period. We have not followed the evolution of the instability further than t=900 s because a significant reflection of vorticity off of the ionosphere would then presumably have occurred. In order to examine this effect, a more realistic boundary condition for the ionosphere would have to be considered. We hope to address this in the future. It should also be pointed out that we have of course neglected to specify a driver for the FLR, and in particular we have not taken into account the fact that compressional MHD energy is being pumped into the resonance. It is possible that this source of energy may offset the dissipation of the FLR by the KHI at the equatorial plane. We are currently addressing this problem, which from a computational point of view is complicated by the fact that the observed azimuthal scale lengths of the excited FLR are considerably larger than the azimuthal wavenumbers corresponding to the KHI. The main purpose of the present work has been to point out that the velocity shears which are seen in the high-latitude ionosphere have possible sources in the equatorial plane of the magnetosphere and that the vorticity which develops can have a profound effect on the time evolution of the FLR. The above results indicate that this is possible.

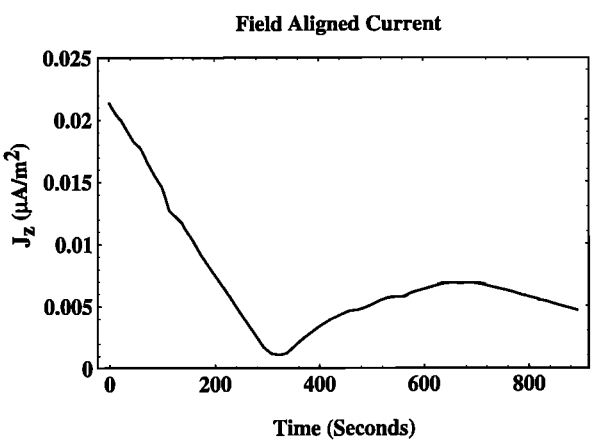

Fig. 14. Maximum modulus of the field-aligned current density J_z near to the ionosphere plotted as a function of time.

CONCLUSION

The results from our three-dimensional simulations of the nonlinear evolution of FLRs show that low frequency (less than approximately 5 mHz) ULF FLRs, with azimuthal fluid velocities of several tens of kilometers per second in the equatorial plane of the Earth's magnetosphere, are likely to be nonlinearly unstable to the KHI. For such velocity fields, the growth times of the KHI are of the order of several tens to hundreds of seconds, which is of the order of half a wave period or less for the lowest frequency ULF resonances. Observations of the velocity fields of FLRs in the auroral E region, and the mapping of these fields to the equatorial plane, indicate that FLRs can typically have oscillating velocity fields with amplitudes near 100 km/s. These high velocities have also been observed in low-frequency (less than 4 mHz) FLRs by the ISEE spacecraft in the outer dawn magnetosphere [*Mitchell et al.*, 1990]. The localized vortex cells which evolve in the equatorial region of the FLR propagate to the ionosphere as shear Alfvén waves, producing vortex cells in the ionosphere even though the FLR is stable to the KHI near the ionosphere. The formation of vortex cells leads to a substantial spatial broadening of the FLR, suggesting that nonlinear effects might play an important role in dissipating the resonance. Consequently, it is important to consider these nonlinear effects when evaluating other damping mechanisms such as absorption due to finite Pedersen conductivity in the ionosphere, and mode conversion to kinetic Alfvén waves which requires a very nar-

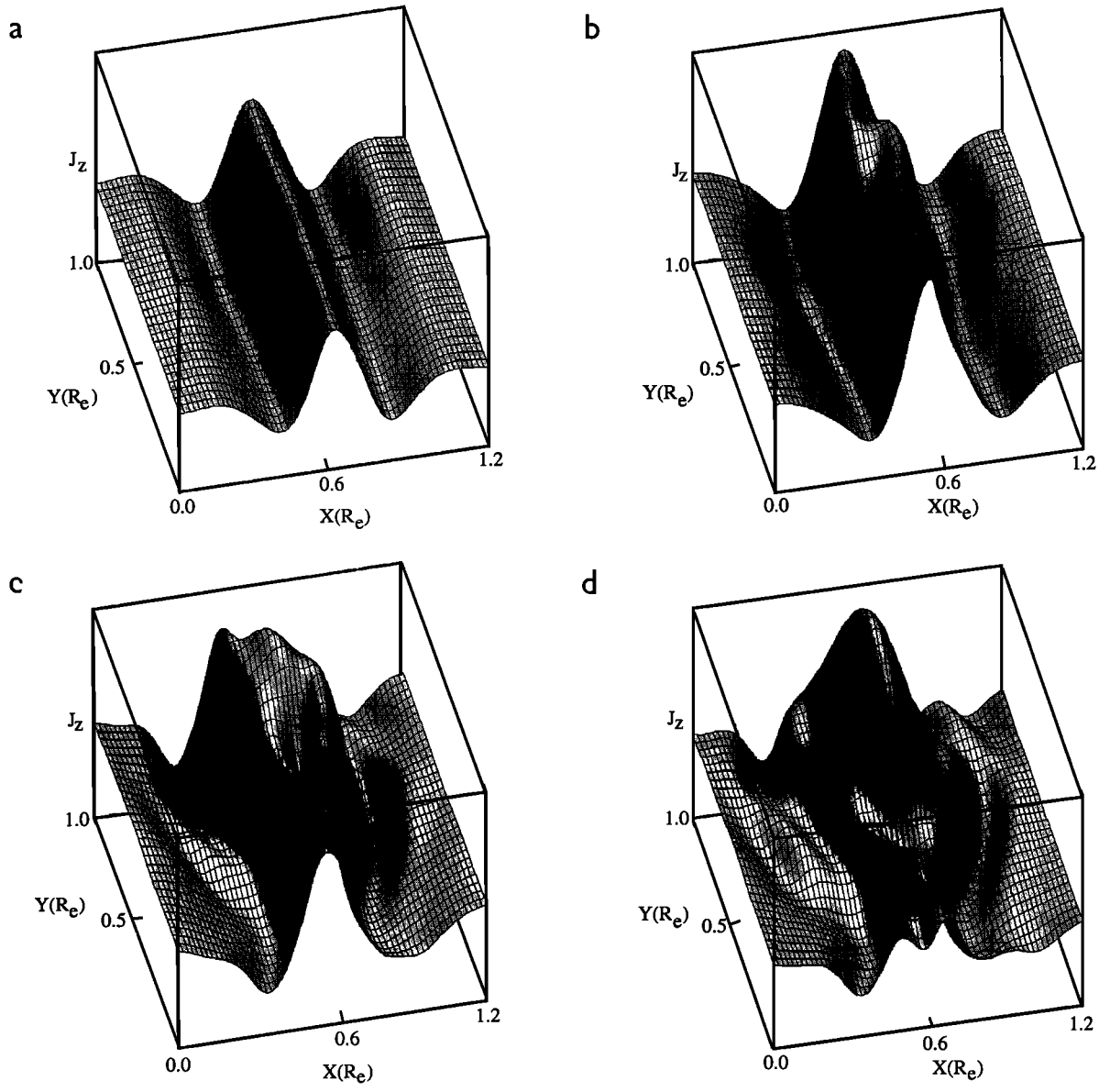

Fig. 15. Evolution of the field-aligned current density (in arbitrary units) in the x-y plane near to the ionosphere. The center of the FLR is situated at 8-10 R_E in the equatorial plane: (a) t=400 s, (b) t=475 s, (c) t=562 s, and (d) t=650 s.

row resonance structure (comparable to the ion gyroradius).

The observational evidence for nonlinear effects in FLRs is still rather limited. *Samson et al.* [1992b] noted that vortex cells in ionospheric *E* region flows can evolve on field lines with existing FLRs (see Figure 2 in this paper). The scale size of these vortex cells is about 10 degrees in longitude, Figure 2*c*, corresponding to approximately 1 to 2 R_E in the equatorial plane. Furthermore, the growth time of the vortex cells is about 100-200 s which is compatible with the growth times determined by our computer model. Note, however, that the vortex cells seen during substorm intensifications always tend to "wrap up" in the same direction, with eastward flows poleward (westward electrojet) and westward flows equatorward (eastward electrojet). This feature is not explained by our computer model. The Ps6 geomagnetic pulsations and vortex flows seen during the substorm recovery phase [*Gustafsson et al.*, 1981; *Rajaram et al.*, 1986] may also be candidates for our nonlinear KHI model. Field lines threading the Ps6 regions in the ionosphere map to radial distances of approximately 7 to 10 R_E in the equatorial region of the dawn and postmidnight magnetosphere [*Pulkkinen et al.*, 1991], which is the region where the low-frequency (1-4 mHz) resonances are seen [*Mitchell et al.*, 1990; *Ruohoniemi et al.*, 1991; *Samson et al.* 1992a, b]. Finally, we note that the FLRs studied by *Mitchell et al.* [1990] have very large velocity fields (100 to 200 km/s). At times the amplitude of the radial component of the velocity they observed was comparable to the azimuthal component, indicating that these velocity fields are not inconsistent with the possible existence of a nonlinear KHI.

Our computational model shows that FLRs should be unstable to the KHI and presumably gives a reasonable approximation of the initial evolution of vortex structures and their propagation to the ionosphere. A more complete treatment of this problem requires realistic ionospheric boundary conditions and a compressional MHD driver for a FLR evolving in a nonuniform magnetoplasma. The coupling of the compressional MHD waves to the shear Alfvén waves will compete with the dissipation of the FLRs by the KHI vortices. We are examining this problem but a number of computa-

tional difficulties arise. In addition to being fully three dimensional, the code and initialization must take into account the differing scale sizes of the KHI compared to those of the FLRs. For example, the FLRs have azimuthal wavelengths of the order of 10-20 R_E, whereas the maximum growth rate of the KHI has wavelengths of the order of 1-2 R_E.

The Cartesian geometry which we are using also does not allow the formation of FAC densities which are large enough to produce nonlinear effects near the ionosphere. In fact, observations of FLRs indicate that current densities of 5 $\mu A/m^{-2}$ can occur close to the ionosphere [*Walker et al.*, 1992]. These current densities are more than adequate to drive current sheet instabilities or, perhaps, tearing mode instabilities [*Seyler*, 1990]. In our computer models, the largest current densities that we observe are of the order of 0.02 $\mu A/m^{-2}$. Taking into account mapping factors, this corresponds to a current density greater than 10 $\mu A/m^{-2}$ at the ionosphere, assuming dipolar magnetic field lines at auroral latitudes. The geometry of dipolar fields will also lead to larger electric fields and flow velocities near to the ionsophere compared to those we have calculated. However, these geometric effects should have little influence on the overall growth rates of the KHI and morphology of the fields of the Alfvén waves. Taking into account the dipole geometry, we find that our results correspond to realistic values for the field-aligned currents and velocity fields near to the ionosphere.

Acknowledgments. This research was supported by the Natural Sciences and Engineering Research Council of Canada (NSERC). We would also like to thank the referees for there many useful comments and suggestions for improvements to the manuscript.

The Editor thanks J. V. Hollweg and J. S. Murphree for their assistance in evaluating this paper.

REFERENCES

Allan, W., and E. M. Poulter, Damping of magnetospheric cavity modes, *J. Geophys. Res., 94*, 11843, 1989.

Allan, W., J. R. Manuel, and E. M. Poulter, Magnetospheric cavity modes: Some nonlinear effects, *J. Geophys. Res., 96*, 11461, 1991.

Anderson, D. V., A. R. Fry, R. Gruber, and A. Roy, Gigaflop speed algorithm for the direct solution of large blocktridiagonal systems in 3D physics applications, *Lawrence Livermore Nat. Lab. Rep. UCRL-96034*, Lawrence Livermore Lab., Livermore, Calif., 1987.

Baker, K. B., and S. Wing, A new magnetic coordinate system for conjugate studies of high latitudes, *J. Geophys. Res., 94*, 9139, 1989.

Briley, W. R., and H. McDonald, Solution of the multidimensional compressible Navier-Stokes equations by a generalized implicit method, *J. Comput. Phys., 24*, 372, 1977

Chen, L., and A. Hasegawa, A theory of long-period magnetic pulsations, 1, Steady excitation of field line resonances, *J. Geophys. Res., 79*, 1024, 1974.

Davis, T. N., and T. J. Hallinan, Auroral Spirals, 1, Observations, *J. Geophys. Res., 81*, 3953, 1976.

Douglas, J., and J. Gunn, A general formulation of alternating direction methods. I. Parabolic and hyperbolic problems, *Numer. Math., 6*, 428, 1964.

Finan, C. H., and J. Killeen, Solution of the time dependent, three dimensional resistive magnetohydrodynamic equations, *Comput. Phys. Commun., 24*, 441, 1981.

Goertz, C. K., Kinetic Alfvén waves on auroral field lines, *Planet. Space Sci., 32*, 1387, 1984.

Gustafsson, G., W. Baumjohan, and I. Iverson, Multi-method observations and modelling of the three-dimensional currents associated with a very strong Ps6 event, *J. Geophys. (Germany), 49*, 138, 1981.

Hallinan, T. J., Auroral spirals, 2, Theory, *J. Geophys. Res. , 81*, 3959, 1976.

Hallinan, T. J., and T. N. Davis, Small scale auroral arc distortions, *Planet. Space Sci., 18*, 1735, 1970.

Hasegawa, A., Particle acceleration by MHD surface wave and formation of aurora, *J. Geophys. Res., 81*, 5083, 1976.

Hollweg, J. V., and G. Yang, Resonace absorption of compressible magnetohydrodynamic waves at thin "surfaces," *J. Geophys. Res., 93*, 5423, 1988.

Mitchell, D. G., M. J. Engebretson, D. J. Williams, C. A. Cattel, and R. Lundin, Pc 5 Pulsations in the outer dawn magnetosphere seen by ISEE 1 and 2, *J. Geophys. Res., 95*, 967, 1990.

Namikawa, T., and H. Hamabata, The α - effect generated by standing Alfvén waves, *J. Plasma Phys., 40*, 353, 1988.

Pulkkinen, T. I., R. J. Pellinen, H. E. J. Koskinen, H. J. Opgenoorth, J. S. Murphree, V. Petrov, A. Zaitsev, and E. Friis-Christensen, Auroral signatures of substorm recovery phase: A case study, in *Magnetospheric Substorms, Geophys. Monogr. Ser.*, vol. 64, edited by J. R. Kan, T. A. Potemra, S. Kokubun, and T. Iijima, pp. 333-341, AGU, Washington, D.C., 1991.

Rajaram, G., G. Rostoker, and J. C. Samson, Wave characteristics of Ps6 magnetic variations and their implications for convective flow in the magnetotail, *Planet. Space. Sci., 34*, 319, 1986.

Ruohoniemi, J. M., R. A. Greenwald, K. B. Baker, and J. C. Samson, HF radar observations of Pc5 field line resonances in the midnight/early morning MLT sector, *J. Geophys. Res., 96*, 15697, 1991.

Samson, J. C., D. D. Wallis, T. J. Hughes, F. Creutzberg, J. M. Ruohoniemi, and R. A. Greenwald, Substorm intensifications and field line resonances in the nightside magnetosphere, *J. Geophys. Res., 97*, 8495-8518, 1992a.

Samson, J. C., B. G. Harrold, J. M. Ruohoniemi, R. A. Greenwald, and A. D. M. Walker, Field line resonances associated with MHD waveguides in the magnetosphere, *Geophys. Res. Lett., 19*, 441, 1992b.

Seyler, C. E., Jr., Nonlinear 3-D evolution of bounded kinetic Alfvén waves due to shear flow and collisionless tearing instability, *Geophys. Res. Lett., 15*, 756, 1988.

Seyler, C. E., A mathematical model of the structure and evolution of small-scale discrete auroral arcs, *J. Geophys. Res., 95*, 17199, 1990.

Shukla, P. K., M. Y. Yu, and R. K. Varma, Drift-Alfvén vortices, *Phys. Fluids, 28*, 1719, 1985.

Southwood, D. J., Some features of field line resonances in the magnetosphere, *Planet. Space Sci., 22*, 483, 1974.

Walker, A. D. M., Modelling of Pc5 pulsation structure in the magnetosphere, *Planet. Space Sci., 28*, 213, 1980.

Walker, A. D. M., The Kelvin-Helmholtz instability in the low-latitude boundary layer, *Planet. Space Sci., 29*, 1119, 1981.

Walker, A. D. M., R. A. Greenwald, W. F. Stuart, and C. A. Green, Stare auroral radar observations pf Pc5 geomagnetic pulsations, *J. Geophys. Res., 84*, 3373, 1979.

Walker, A. D. M., J. M. Ruohoniemi, K. B. Baker, R. A. Greenwald, and J. C. Samson, Spatial and temporal behavior of ULF pulsations observed by the Goose Bay HF radar, *J. Geophys. Res., 97*, 12187-12202, 1992.

P. Frycz, B. G. Harrold, R. Rankin, and J. C. Samson, Canadian Network for Space Research, Biological Sciences Building, CW-005, University of Alberta, Canada T6G 2E9.

(Received April 23, 1992;
revised June 29, 1992;
accepted June 29, 1992.)